PCCP

Cross-polarization for a fluoropolymer involving multiple spin baths of abundant nuclei

Paul Hazendonk,[a] Robin K. Harris,*[a] Giancarlo Galli[b] and Silvia Pizzanelli[b]

[a] *Department of Chemistry, University of Durham, South Road, Durham, UK DH1 3LE. E-mail: R.K.Harris@Durham.ac.uk; Fax: +44 191 384-4737; Tel: +44 191 374 3121*

[b] *Dipartimento di Chimica e Chimica Industriale, Università di Pisa, via Risorgimento 35-56126 Pisa, Italy*

Received 5th October 2001, Accepted 8th November 2001
First published as an Advance Article on the web 18th January 2002

The thermodynamic theory of cross-polarization (CP) between one abundant and one rare spin is well understood and widely applied. CP dynamics between several abundant spin baths has some inherent complications that lead to misinterpretation of the CP rates and relaxation parameters if not properly accounted for. A general thermodynamic description of CP dynamics involving up to six spin baths is developed and implemented with MATLAB. The CP dynamics for a fluorinated polymer, (2-perfluorohexylethyl acrylate)–styrene co-polymer, was analysed as a system with five spin baths—four ^{19}F and one ^{1}H. The CP behaviour was successfully simulated above the glass-transition temperature. The CP rates and $T_{1\rho}$'s are discussed in terms of the structure and dynamic behaviour of the polymer.

Introduction

Solid-state NMR spectroscopy of fluoropolymers presents a situation where the nuclides involved, ^{1}H and ^{19}F, are isotopically abundant and possess strong magnetic moments. In the more usual situation, when studying NMR of solid polymers, one has one abundant strong nucleus and one rare weak nucleus, namely proton and carbon, respectively. Thus, when considering experiments involving two abundant strong spin types, adjustments have to be made to both the experimental design and the theoretical approaches.[1–3]

The Larmor frequencies of ^{19}F and ^{1}H are 6% apart, so modifications to the conventional probe circuit design are required to isolate the two channels sufficiently at high powers. This problem may be overcome in various ways, so that now experiments such as $\{^{1}H\}$–^{19}F and $\{^{19}F\}$–^{1}H cross-polarization (observing ^{19}F whilst decoupling ^{1}H and *vice versa*) have become routine.[4,5] Before this was possible most NMR studies of solid fluoropolymers were restricted to combined rotation and multiple pulse spectroscopy (CRAMPS) and/or wide-line spectra of perfluorinated materials.[6,7]

Many fluoropolymers are semicrystalline, *i.e.* they have both crystalline and amorphous domains. NMR can be used to study both, whilst X-ray diffraction methods are only suited to examining the crystalline domains. Other physical methods do not generally give information at the molecular level but rather offer insight only into the bulk properties of the material. NMR is extremely sensitive to subtle differences in local electronic environments. Thus separate signals for the crystalline and amorphous domains can be obtained by the use of appropriate pulse sequences.[8]

NMR can be used to study not only the chemical and physical structure of solid polymers, but also dynamic processes, such as main-chain and side-chain motions. Characterising these processes can give valuable insight into the bulk properties of these polymers. For example the ferroelectric, piezoelectric and pyroelectric properties of fluoropolymers are related to the existence of polar and non-polar crystalline forms.[7,9] Studies of dynamics require measurements of rotating frame, spin–spin, and spin–lattice relaxation times over a wide temperature range.

Cross-polarization (CP) dynamics can provide valuable information on both structure and dynamics.[10–13] However, obtaining CP parameters in the (H,F) case is complicated since the second nuclide now has to be considered as abundant and possessing a strong magnetic moment. The CP curves still resemble those of the abundant-rare spin case. However, the parameters cannot be obtained directly from the curves. The latter have to be characterized in terms of "effective" cross-polarization and rotating-frame-relaxation rates. These parameters are related to the "true" cross-polarization and rotating-frame-relaxation rates in a complicated way. Thus, in general the CP dynamics of systems containing multiple abundant nuclei have to be simulated numerically in order to extract the "true" CP parameters. Analytical solutions exist only for the case of two spin baths.[2,3] Fluoropolymer systems often consist of several spin baths, so that a general approach has to be devised to study their CP dynamics. This arises because, under the magic-angle spinning (MAS) conditions of the experiments, resonances from non-equivalent fluorines are resolved and therefore the ^{19}F magnetization cannot be treated as homogeneous.

In this study a simple thermodynamic theory of CP is generalised to an arbitrary number of spin baths, and is applied to a polymer system, –[CH(C_6H_5)CH_2]$_x$–[CH_2CH(C(=O)OC_2H_4-C_6F_{13})]$_y$–, referred to here by the abbreviation, copoly(**I**) (see Scheme 1). This is essentially a random copolymer of styrene and 2-perfluorohexylethyl acrylate. It has four resolved lines in the ^{19}F spectrum, and thus the ^{1}H to ^{19}F CP (and *vice versa*) is suitable for a treatment involving five spin baths.

Recently, several poly(fluoroalkyl acrylate) and methacrylate polymers have been developed, and their physico-chemical and structural properties have been intensively studied.[14–16]

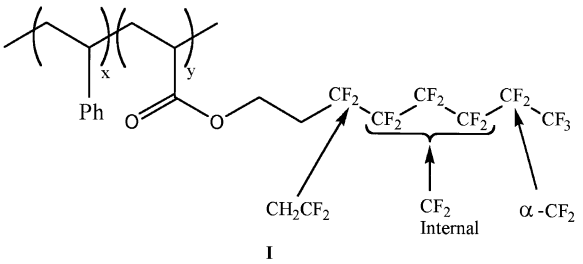

I

Scheme 1

These materials are transparent, have low surface tension and low refractive index. These properties make them attractive systems for industrial applications in, for instance, optical fibres, moisture-proof coatings, and oil and water repellent agents.[15] Copolymers containing the monomers perfluoroalkyl acrylate and styrene have been synthesized, and found to exhibit properties that can be tuned through variation of the chemical composition.[16] In particular, styrene-rich copolymers are completely amorphous and thus able to form transparent films and thin layers by spin-coating or spraying solutions.

Theory

The phenomenological spin thermodynamics theory describing cross-polarization between two abundant spin reservoirs based on the spin temperature hypothesis is[2,3] extended herein to an arbitrary number of spin baths. All spins are subject to the Zeeman interaction in a magnetic field $\boldsymbol{B}_0$, are assumed to be abundant, and have the same quantum number (*i.e.* 1/2). The magnetization, $\boldsymbol{M}$, and energy, E, for each spin-bath can be expressed as:

$$\boldsymbol{M} = \frac{\hbar}{kT}\frac{1}{3} N \cdot I(I+1)\gamma^2\hbar \cdot \boldsymbol{B}_0 = \beta \cdot C \cdot \boldsymbol{B}_0 \qquad (1)$$

$$E = -\frac{\hbar}{kT}\frac{1}{3} N \cdot I(I+1)\gamma^2\hbar \cdot \boldsymbol{B}_0^2 = -\beta \cdot C \cdot \boldsymbol{B}_0^2 \qquad (2)$$

where T is the spin temperature, I is the spin quantum number, N is the spin number density, γ is the gyromagnetic ratio, and $C = NI(I+1)\gamma^2\hbar/3$ is the Curie constant. The property β, defined as $\hbar/kT$, is the inverse spin temperature. It is proportional to the magnetization when only the Zeeman interaction is considered in the high temperature approximation.

Take N isolated spin reservoirs with total energy

$$E = E_1 + E_2 + \cdots + E_N . \qquad (3)$$

When the spins are isolated from the lattice, and relaxation is ignored, energy is conserved, so

$$\frac{\mathrm{d}}{\mathrm{d}t}E = \frac{\mathrm{d}}{\mathrm{d}t}E_1 + \frac{\mathrm{d}}{\mathrm{d}t}E_2 + \cdots + \frac{\mathrm{d}}{\mathrm{d}t}E_N = 0.^3 \qquad (4)$$

Assuming that the exchange of spin energy between spin reservoirs obeys first-order kinetics, the CP dynamics is described by the following set of differential equations

$$\begin{aligned}
\frac{\mathrm{d}}{\mathrm{d}t}E_1 &= +\frac{1}{T_{11}}E_1 + \frac{1}{T_{21}}E_2 + \frac{1}{T_{31}}E_3 + \cdots + \frac{1}{T_{N1}}E_N \\
\frac{\mathrm{d}}{\mathrm{d}t}E_2 &= +\frac{1}{T_{12}}E_1 + \frac{1}{T_{22}}E_2 + \frac{1}{T_{32}}E_3 + \cdots + \frac{1}{T_{N2}}E_N \\
\frac{\mathrm{d}}{\mathrm{d}t}E_3 &= +\frac{1}{T_{13}}E_1 + \frac{1}{T_{23}}E_2 + \frac{1}{T_{33}}E_3 + \cdots + \frac{1}{T_{N3}}E_N \\
&\vdots \qquad \vdots \qquad \vdots \qquad \vdots \qquad \vdots \\
\frac{\mathrm{d}}{\mathrm{d}t}E_N &= +\frac{1}{T_{1N}}E_1 + \frac{1}{T_{2N}}E_2 + \frac{1}{T_{3N}}E_3 + \cdots + \frac{1}{T_{NN}}E_N
\end{aligned} \qquad (5)$$

where $1/T_{ij}$ describes the characteristic transfer time from the ith to the jth reservoir.

Conservation of energy requires that the coefficients sum to zero column-wise. In other words

$$\begin{aligned}
\frac{1}{T_{11}} &= -\frac{1}{T_{12}} - \frac{1}{T_{13}} - \cdots - \frac{1}{T_{1N}} \\
\frac{1}{T_{22}} &= -\frac{1}{T_{21}} - \frac{1}{T_{23}} - \cdots - \frac{1}{T_{2N}} \\
\frac{1}{T_{33}} &= -\frac{1}{T_{31}} - \frac{1}{T_{32}} - \cdots - \frac{1}{T_{3N}} \\
&\vdots \qquad \vdots \qquad \vdots \qquad \vdots \\
\frac{1}{T_{NN}} &= -\frac{1}{T_{N1}} - \frac{1}{T_{N2}} - \cdots - \frac{1}{T_{NN-1}}
\end{aligned} \qquad (6)$$

The forward and reverse rates are proportioned according to their corresponding equilibrium energies, resulting in

$$\frac{E_1^{\mathrm{eq}}}{T_{12}} = \frac{E_2^{\mathrm{eq}}}{T_{21}}, \frac{E_1^{\mathrm{eq}}}{T_{13}} = \frac{E_3^{\mathrm{eq}}}{T_{31}}, \ldots, \frac{E_1^{\mathrm{eq}}}{T_{1N}} = \frac{E_N^{\mathrm{eq}}}{T_{N1}} \qquad (7)$$

The equilibrium energies are given by eqn. (2), at some given equilibrium spin temperature, T_{eq}, and magnetic field, $\boldsymbol{B}_1$. Under Hartman–Hahn matching conditions, where each spin bath is irradiated according to $\gamma_1\boldsymbol{B}_1 = \gamma_2\boldsymbol{B}_2 = \cdots = \gamma_N\boldsymbol{B}_N$, the ratios of the equilibrium energies become

$$\frac{E_1^{\mathrm{eq}}}{E_2^{\mathrm{eq}}} = \frac{[N_1(I_1(I_1+1))\gamma_1^2\boldsymbol{B}_{11}^2]/T_{\mathrm{eq}}}{[N_2(I_2(I_2+1))\gamma_2^2\boldsymbol{B}_{12}^2]/T_{\mathrm{eq}}} = \frac{N_1}{N_2} = \varepsilon_{12} \qquad (8)$$

when $I_1 = I_2$. Consequently

$$\frac{\varepsilon_{12}}{T_{12}} = \frac{1}{T_{21}}, \frac{\varepsilon_{13}}{T_{13}} = \frac{1}{T_{31}}, \ldots, \frac{\varepsilon_{1N}}{T_{1N}} = \frac{1}{T_{N1}}. \qquad (9)$$

Consideration of eqn. (9) and (6) means that the set of differential equations, eqn. (5), can be re-expressed as

$$\begin{aligned}
\frac{\mathrm{d}}{\mathrm{d}t}E_1 &= \frac{1}{T_{12}}[\varepsilon_{12}E_2 - E_1] + \frac{1}{T_{13}}[\varepsilon_{13}E_3 - E_1] + \cdots + \frac{1}{T_{1N}}[\varepsilon_{1N}E_N - E_1] \\
\frac{\mathrm{d}}{\mathrm{d}t}E_2 &= \frac{1}{T_{12}}[E_1 - \varepsilon_{12}E_2] + \frac{1}{T_{23}}[\varepsilon_{23}E_3 - E_2] + \cdots + \frac{1}{T_{2N}}[\varepsilon_{2N}E_N - E_2] \\
\frac{\mathrm{d}}{\mathrm{d}t}E_3 &= \frac{1}{T_{13}}[E_1 - \varepsilon_{13}E_3] + \frac{1}{T_{23}}[E_2 - \varepsilon_{23}E_3] + \cdots + \frac{1}{T_{3N}}[\varepsilon_{3N}E_N - E_3] \\
&\vdots \qquad\qquad \vdots \qquad\qquad \vdots \qquad\qquad \vdots \\
\frac{\mathrm{d}}{\mathrm{d}t}E_N &= \frac{1}{T_{1N}}[E_1 - \varepsilon_{1N}E_N] + \frac{1}{T_{2N}}[E_2 - \varepsilon_{2N}E_N] + \cdots + \frac{1}{T_{N-1N}}[E_{N-1} - \varepsilon_{N-1N}E_N]
\end{aligned} \qquad (10)$$

In matrix form, eqn. (10) is $\frac{d}{dt}\boldsymbol{E}=\boldsymbol{M}\cdot\boldsymbol{E}$ where the matrix $\boldsymbol{M}$ is given by:

$$\begin{bmatrix} -\frac{1}{T_{12}}-\frac{1}{T_{13}}-\cdots-\frac{1}{T_{1N}} & \frac{\varepsilon_{12}}{T_{12}} & \frac{\varepsilon_{13}}{T_{12}} & \cdots & \frac{\varepsilon_{1N}}{T_{1N}} \\ \frac{1}{T_{12}} & -\frac{\varepsilon_{12}}{T_{12}}-\frac{1}{T_{23}}-\cdots-\frac{1}{T_{2N}} & \frac{\varepsilon_{23}}{T_{23}} & \cdots & \frac{\varepsilon_{2N}}{T_{2N}} \\ \frac{1}{T_{13}} & \frac{1}{T_{23}} & -\frac{\varepsilon_{13}}{T_{13}}-\frac{\varepsilon_{23}}{T_{23}}-\cdots-\frac{1}{T_{3N}} & \cdots & \frac{\varepsilon_{3N}}{T_{3N}} \\ \vdots & \vdots & \vdots & \ddots & \vdots \\ \frac{1}{T_{1N}} & \frac{1}{T_{2N}} & \frac{1}{T_{3N}} & \cdots & -\frac{\varepsilon_{1N}}{T_{1N}}-\frac{\varepsilon_{2N}}{T_{2N}}+\cdots+\frac{\varepsilon_{N-1N}}{T_{N-1N}} \end{bmatrix} \quad (11)$$

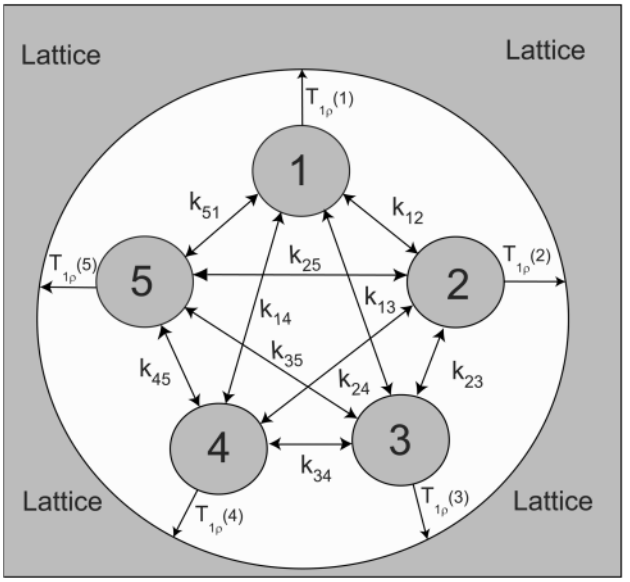

Fig. 1 The model of five spin baths used to simulate the cross-polarization dynamics of copoly(**I**). Each spin bath is characterized by a relative population, ε, and an inverse spin temperature, β.

The polarization transfer between the spin baths during the irradiation may be described in terms of their inverse spin temperatures.[2] Spins in separate baths with inverse spin temperatures, β_i, β_j, *etc.*, are in contact with each other and to the lattice as seen in Fig. 1. The lattice is assumed to have an infinite heat capacity, and thus stays at a constant inverse spin temperature β_L. The spin baths have comparable finite heat capacities. *Via* eqn. (2), the set of differential equations, eqn. (10), becomes, in terms of spin temperatures:

$$\begin{aligned} \frac{d}{dt}\beta_1 &= \frac{1}{T_{12}}[\beta_2-\beta_1]+\frac{1}{T_{13}}[\beta_3-\beta_1]+\cdots+\frac{1}{T_{1N}}[\beta_N-\beta_1] \\ \frac{d}{dt}\beta_2 &= \frac{\varepsilon_{12}}{T_{12}}[\beta_1-\beta_2]+\frac{1}{T_{23}}[\beta_3-\beta_2]+\cdots+\frac{1}{T_{2N}}[\beta_N-\beta_2] \\ \frac{d}{dt}\beta_3 &= \frac{\varepsilon_{13}}{T_{13}}[\beta_1-\beta_3]+\frac{\varepsilon_{23}}{T_{23}}[\beta_2-\beta_3]+\cdots+\frac{1}{T_{3N}}[\beta_N-\beta_3] \\ &\vdots \qquad\qquad \vdots \qquad\qquad \vdots \qquad\qquad \vdots \\ \frac{d}{dt}\beta_N &= \frac{\varepsilon_{1N}}{T_{1N}}[\beta_1-\beta_N]+\frac{\varepsilon_{2N}}{T_{2N}}[\beta_2-\beta_N]+\cdots+\frac{\varepsilon_{N-1N}}{T_{N-1N}}[\beta_{N-1}-\beta_N] \end{aligned} \quad (12)$$

Including relaxation in the rotating frame, the differential equations in eqn. (12) become, in matrix form, $\frac{d}{dt}\boldsymbol{Q}=(\boldsymbol{M}'-\boldsymbol{R})\cdot\boldsymbol{Q}$, where $\boldsymbol{Q}=[\beta_A, \beta_B, \beta_C, \ldots, \beta_N]^T$, $\boldsymbol{R}$ is a diagonal matrix containing the rotating-frame-relaxation rates, and $\boldsymbol{M}'$ is the matrix:

$$\begin{bmatrix} -\frac{1}{T_{12}}-\frac{1}{T_{13}}-\cdots-\frac{1}{T_{1N}} & \frac{1}{T_{12}} & \frac{1}{T_{13}} & \cdots & \frac{1}{T_{1N}} \\ \frac{\varepsilon_{12}}{T_{12}} & -\frac{\varepsilon_{12}}{T_{12}}-\frac{1}{T_{23}}-\cdots-\frac{1}{T_{2N}} & \frac{1}{T_{23}} & \cdots & \frac{1}{T_{2N}} \\ \frac{\varepsilon_{13}}{T_{13}} & \frac{\varepsilon_{23}}{T_{23}} & -\frac{\varepsilon_{13}}{T_{13}}-\frac{\varepsilon_{23}}{T_{23}}-\cdots-\frac{1}{T_{3N}} & \cdots & \frac{1}{T_{3N}} \\ \vdots & \vdots & \vdots & \ddots & \vdots \\ \frac{\varepsilon_{1N}}{T_{1N}} & \frac{\varepsilon_{2N}}{T_{2N}} & \frac{\varepsilon_{3N}}{T_{3N}} & \cdots & -\frac{\varepsilon_{1N}}{T_{1N}}-\frac{\varepsilon_{2N}}{T_{2N}}+\cdots+\frac{\varepsilon_{N-1N}}{T_{N-1N}} \end{bmatrix} \quad (13)$$

This system of equations can be solved as $\boldsymbol{Q}(t)=[\exp(\boldsymbol{M}'-\boldsymbol{R})t]\cdot\boldsymbol{Q}(0)$, where $\exp(\boldsymbol{M}'-\boldsymbol{R})$ can be evaluated as $\boldsymbol{\Lambda}^{-1}\cdot\exp(\boldsymbol{D})\cdot\boldsymbol{\Lambda}$, with $\boldsymbol{D}$ as the matrix of eigenvalues and $\boldsymbol{\Lambda}$ as the matrix of eigenvectors.

Experimental

Preparation of copoly(I)

2-Perfluorohexylethyl acrylate was prepared by an esterification reaction of acryloyl chloride and 2-perfluorohexylethanol; Acryloyl chloride (35 mmol) was added dropwise to a solution of 2-perfluorohexylethanol (27 mmol), triethylamine (54 mmol) and 2,6-di-*tert*-butyl-4-cresol (15 mg) in anhydrous diethyl ether (200 ml) under an inert atmosphere at 0 °C. After stirring for 16 h at ambient temperature, the reaction mixture was washed with 5% HCl, 5% $NaHCO_3$ and water. The organic phase was dried over Na_2SO_4, the solvent was removed *in vacuo* and the liquid residue was distilled at reduced pressure to give the monomer (yield 85%): bp 50 °C (0.2 mmHg). ^{1}H NMR ($CDCl_3$): δ 6.5 (d, 1H) (CH-*cis*), 6.2 (dd, 1H) (CH-*gem*), 5.8 (d, 1H) (CH-*trans*), 4.5 (t, 2H) (CH_2–OOC), 2.5 (m, 2H) (CH_2CF_2).

The 2-perfluorohexylethyl acrylate and styrene copolymer, copoly(**I**), was prepared by free radical polymerisation: A solution of 2-perfluorohexylethyl acrylate (1.37 mmol), styrene (4.06 mmol) and α,α'-azobisisobutyronitrile (AIBN) (10 mg) in anhydrous benzene (5 ml) was sealed in a Pyrex tube after degassing by repeated freeze–thaw cycles. The polymerisation was then conducted at 60 °C for 72 h. The crude product was purified by precipitation from $CHCl_3$–MeOH solutions; the precipitated polymer was filtered and dried *in vacuo* (yield 72%). ^{1}H NMR: ($CDCl_3$) δ 7.5–6.4 ppm (broad signal, 3.5H) (phenyl), 4.4–3.4 ppm (broad signal, 0.6H) (CH_2–OOC), 2.5–0.2 ppm (m, 3.6H) (CH_2–CF_2 and CH, CH_2 of the polymeric chain).

The copolymer is characterised by a composition of styrenic units equal to 70%, $M_n=13.6\times10^3$ and $M_w/M_n=1.6$. It shows a glass transition at 45 °C. The average numbers of styrenic and acrylic units, x and y, are 48 and 20 respectively, based on the average molecular weight. Proton solution-state NMR spectra were recorded at ambient temperature using a Varian Gemini 200 MHz spectrometer. The chemical shifts are reported with respect to the signal for tetramethylsilane (TMS). The molar mass data were obtained by gel permeation chromatography (GPC) on a Jasco PU-1580 chromatograph with PL gel 5 mm MIXED-C columns connected in series. The system has a Jasco 830-RI refractive index detector and a Perkin-Elmer LC75 spectrophotometric detector. Polystyrene

standards were used for the calibration. Differential scanning calorimetry analyses were performed on a Mettler DCS 30 with a 10 °C min^{-1} heating rate.

Solid-state nuclear magnetic resonance

Solid-state NMR experiments were carried out on a Varian Unity 300 spectrometer operating at 282.21 MHz for ^{19}F and 299.96 MHz for ^{1}H. A Doty Scientific XC (crossed coil) MAS probe double-tuned to ^{1}H and ^{19}F, capable of high-power heteronuclear decoupling (*ca.* 80 kHz) and equipped with silicon nitride 5 mm od rotors, was used. Vespel drive tips and end caps were employed to suppress any unwanted background signal from the fluorine channel, which should be minimal because of the use of ^{1}H–^{19}F cross-polarization. To reduce the effect of rf inhomogeneities over the sample, the volume was restricted to 70 μl in an aurum rotor insert, which was kept in place by the end caps using a PVC plug as a spacer. Rotor speeds were kept in the 15 kHz range. Experiments were performed at 45 and 75 °C. Temperatures were calibrated using the frequency separation between the two signals in the proton spectrum of methanol. The ^{19}F chemical shifts are quoted with respect to the signal of $CFCl_3$, obtained indirectly *via* the fluorine signal of C_6F_6 at −166.4 ppm. Proton chemical shifts were directly referenced with respect to TMS at 0 ppm.

Fluorine-19 MAS NMR spectra were obtained using 3.6 μs (π/2) pulses and recycle delays of 4 s (which are long with respect to the T_1 relaxation times of ^{19}F and ^{1}H). The pulse sequences used for the variable contact time $^{1}H \rightarrow {}^{19}F$ CP measurements, and for the variable spin-lock time measurements of ^{19}F and ^{1}H $T_{1\rho}$ are shown in Fig. 2, the rf power remaining the same throughout the sequence in each channel. In the CP experiment the contact time was varied and the relevant integrated intensities were measured by deconvolution. The cross-polarization experiments were done by matching on the centre-band. The rotating-frame-relaxation time measurements start by creating either a proton or a fluorine magnetization *via* CP, which in turn is locked in the rotating frame for a variable time. Both methods employ fluorine detection. Thus $T_{1\rho}$ for ^{1}H requires a final CP step to ^{19}F with a fixed contact time.

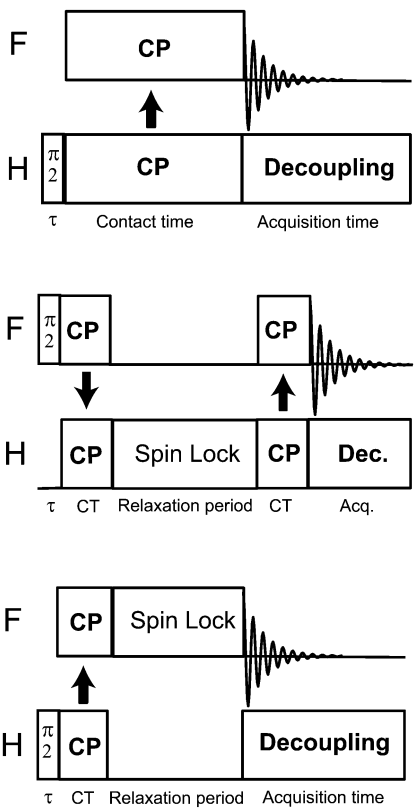

Fig. 2 Pulse sequences used for variable contact time $\{^{1}H\}$–^{19}F cross-polarization (top), ^{19}F detected ^{1}H rotating-frame-relaxation time (middle), and ^{19}F rotating-frame-relaxation time measurements (bottom).

Simulation of CP dynamics

The theory of CP dynamics involving five spin baths was implemented in the MATLAB programming environment. The calculations were based on the model shown in Fig. 1. Each ^{19}F spin bath is characterized with a population relative to the single proton bath, an inverse spin temperature, a rotating-frame spin–lattice relaxation time, a cross-polarization rate with the proton spin bath, and spin-diffusion rates with the other fluorine spin baths. The only other variables were the ^{1}H rotating-frame relaxation-time and initial spin temperature. The ^{1}H and ^{19}F $T_{1\rho}$ values, separately measured, were used as constraints while the CP rates were optimised using a multi-parameter non-linear least-squares optimisation routine based on the Levenberg–Marquardt algorithm.[17] Since no dipolar oscillations were observed in the CP curves no attempt was made to include them in the simulation.[13]

Results

The $\{^{1}H\}$–^{19}F CPMAS NMR spectrum of copoly(**I**) is shown in Fig. 3. Four centre band resonances can be observed, at chemical shifts of −82.6, −114.1, −123.1 and −127.0 ppm, though the last three are not fully resolved. The corresponding full widths at half height are 550, 1340, 1030, and 610 Hz respectively. The assignments are indicated in Fig. 3. The band at −123.1 ppm contains the unresolved resonances from the ^{19}F nuclei of the three central CF_2 groups, which will be treated as forming a single spin bath. $T_{1\rho}$ data for both ^{19}F and ^{1}H nuclei are tabulated in Table 1. The spectra of the ^{1}H–^{19}F CP arrays were deconvolved, giving separate CP curves for the four ^{19}F spin baths. The resulting CP curves are shown in

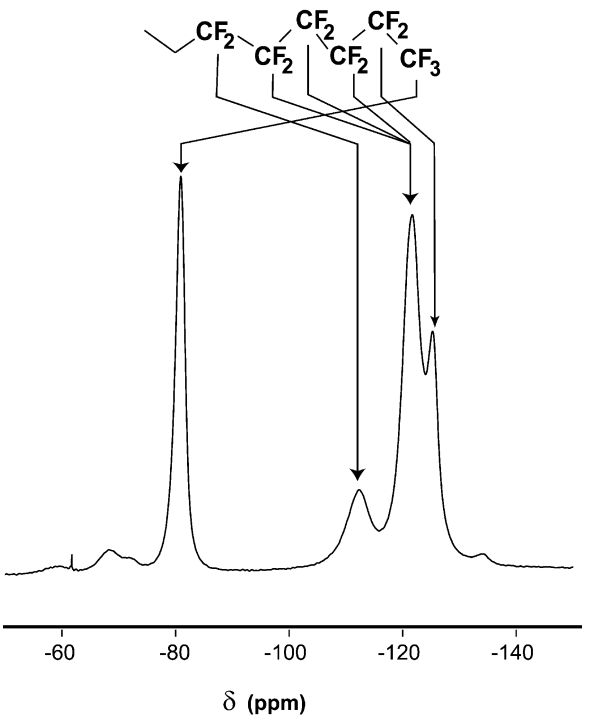

Fig. 3 282 MHz ^{19}F MAS spectrum of copoly(**I**) at 348 K. The assignment to the side-chain fluorines is indicated above.

Table 1 Rotating-frame relaxation times of ^{19}F and ^{1}H nuclei (in both cases fluorine-detected) in copoly(**I**) above the glass transition at 348 K

	–$CH_2\underline{C}F_2$–	–$\underline{C}F_2$ $CF_2\underline{C}F_2$–	–$CF_2\underline{C}F_3$	–$\underline{C}F_3$
$T_{1\rho}$ (F)/(ms)	1.98	1.74	1.46	6.03
St. Dev./(ms)	0.06	0.04	0.10	0.04
$T_{1\rho}$ (H)/(ms)	2.89	2.95	2.71	2.67
St. Dev./(ms)	0.04	0.10	0.03	0.07

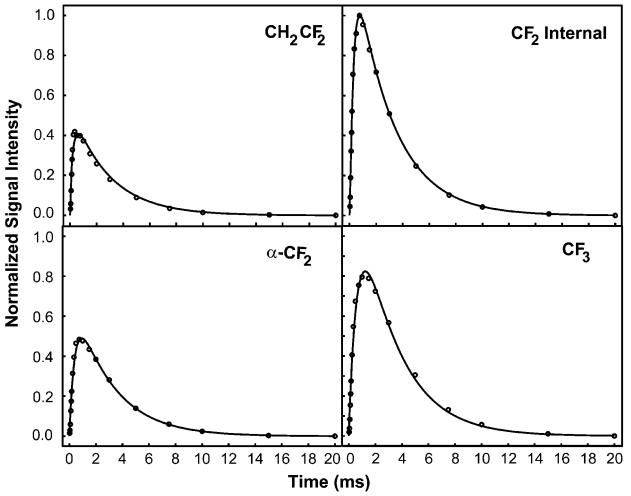

Fig. 4 Experimental and simulated cross-polarization curves of copoly(**I**). The integral of each fluorine signal is plotted as a function of contact time. The type of fluorine environment is indicated in the top right-hand corner. The circles represent the data, the lines are the results of the CP simulations.

Fig. 4. The simulated (fitted) curves are also to be seen in Fig. 4. Table 2 gives the population data for the spin baths arising from the calculations and the cross-polarization rates (with standard deviations). The ^{19}F–^{19}F spin-diffusion rates are tabulated in Table 3. Fig. 5 summarises the CP parameters schematically. Table 4 shows the statistical correlation between the CP rates and the ^{19}F–^{19}F spin-diffusion rates.

Discussion

The copoly(**I**) resonances of CF_3, α-CF_2, and CF_2(internal) are very similar to their counterparts in *n*-perfluoroeicosane, which have chemical shifts of −84, −123, and −128 ppm,

Table 2 Epsilon values,[a] spin bath populations and cross-polarization time constants between the proton and fluorine spin baths

	–$CH_2\underline{C}F_2$–	–$\underline{C}F_2$ $CF_2\underline{C}F_2$–	–$CF_2\underline{C}F_3$	–$\underline{C}F_3$
ε	0.060	0.097	0.071	0.092
St. Dev.	0.001	0.001	0.001	0.001
Pop. (%)	4.5	7.3	5.4	7.0
Forward[b]/(ms)	3.87	8.36	9.56	10.27
St. Dev.	0.02	0.07	0.04	0.03
Reverse[c]/(ms)	0.230	0.806	0.681	0.949
St. Dev.	0.001	0.007	0.003	0.003

[a] ε = effective ratio of fluorine spins to proton spins. [b] Forward process implies CP from the proton to the fluorine spin bath indicated. [c] Reverse process implies CP from the indicated fluorine to the proton spin bath. The forward and reverse values are related by ε as in eqn. (9).

Table 3 Spin-diffusion times between the fluorine spin baths

	–$CH_2\underline{C}F_2$–	–$\underline{C}F_2$ $CF_2\underline{C}F_2$–	–$CF_2\underline{C}F_3$	–$\underline{C}F_3$
–$CH_2\underline{C}F_2$–	xxxxxx[a]	0.154	xxxxxx	xxxxxx
Std. Dev.	xxxxxx	0.003	xxxxxx	xxxxxx
–$\underline{C}F_2$ $CF_2\underline{C}F_2$–	0.250[b]	xxxxxx	1.122	xxxxxx
Std. Dev.	0.005	xxxxxx	0.040	xxxxxx
–$CF_2\underline{C}F_3$	xxxxxx	1.346	xxxxxx	2.159
Std. Dev.	xxxxxx	0.050	xxxxxx	0.080
–$\underline{C}F_3$	xxxxxx	xxxxxx	1.658	xxxxxx
Std. Dev.	xxxxxx	xxxxxx	0.060	xxxxxx

[a] The crosses indicate that these spin-diffusion rates were not included in the simulation. [b] All values are given in ms.

respectively.[18] The remaining –CH_2CF_2– resonance, at −114.1 ppm, has no analogue in *n*-perfluoroeicosane. This resonance is comparable to the defect peaks in poly(vinylidene difluoride) (PVDF) occurring at −113.9 and −116.2 ppm.[13] It falls near the range of the CF_2 (tail, T) resonances in Viton adjacent to a CH_2 (head, H). These are the THTTX resonances, in the range of −108 to −112 ppm[10] and THTTH, THTHH and HTTXH at −114.3, −114.3 and −118.1 ppm, respectively.

The rotating-frame spin–lattice relaxation times of the protons, measured *via* ^{19}F resonances, are the same within experimental error from every fluorine environment (see Table 1). This fact suggests that spin diffusion amongst the protons is efficient, despite the elevated temperature and considerable MAS spin rate, *ca.* 15 kHz. The rotating-frame spin–lattice relaxation times of the fluorine peaks exhibit more differentiation, ranging from 1.49 ms for α-CF_2 to 6.03 ms for CF_3, suggesting that spin diffusion is not very efficient, which is largely due to the high resolution in the ^{19}F spectrum. The long value for CF_3 is at least in part the result of rapid internal rotation about the relevant C–C bond. Assuming rapid rotation with respect to side-chain and backbone motion and that relaxation is dominated by the contribution arising from dipole– dipole interactions, the correlation time is reduced by a factor $(3\cos^2\Delta - 1)/4$. The angle Δ is that between the rotation axis and the F–F vector, which is 90° for a CF_3 group, resulting in a scaling factor of 1/4. Since there are two possible F–F interactions in a CF_3 and only one in CF_2 groups, their rotating-frame relaxation times are expected to have a ratio,

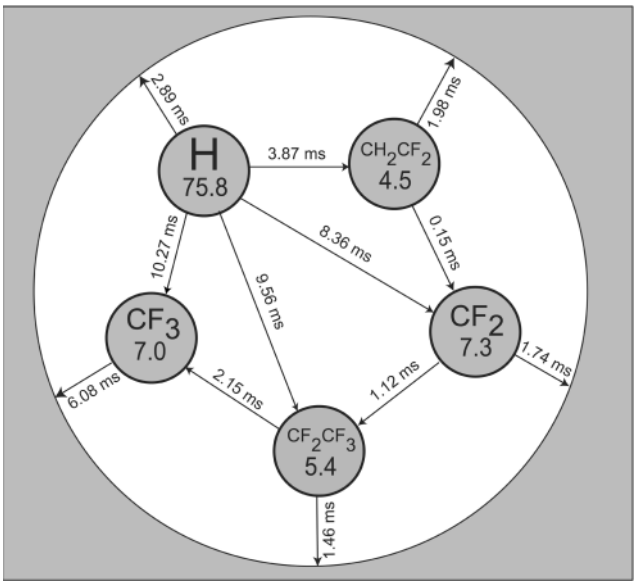

Fig. 5 The experimental cross-polarization and rotating-frame-relaxation times of copoly(**I**) indicated in the five-spin-bath model. The spin-bath populations are also given (in %) for each bath.

Table 4 Correlation coefficients between the CP dynamics parameters

	–CH_2CF_2– H	–$CF_2CF_2CF_2$– H	–CF_2CF_3 H	–CF_3 H	–CH_2CF_2– –$CF_2F_2CF_2$–	–CF_2 CF_2CF_2– –CF_2CF_3
–$CF_2CF_2CF_2$– H	−0.82	1				
–CF_2CF_3 H	−0.03	0.02	1			
–CF_3 H	−0.48	0.02	−0.29	1		
–CH_2CF_2– –CF_2 CF_2CF_2–	0.69	−0.93	−0.04	−0.01	1	
–CF_2 CF_2CF_2– –CF_2CF_3	0.22	−0.20	−0.05	−0.05	0.16	1
–CF_2CF_3 –CF_3	0.06	−0.03	0.35	−0.78	0.02	0.05

$T_{1\rho}(CF_3)/T_{1\rho}(CF_2)$ of approximately 2. In the present case this ratio is larger, ranging between 3 and 4, suggesting that the CF_3 fluorines are more isolated than those in CF_2.

Values of $T_{1\rho}$(F) measured for Viton are shorter than for copoly(**I**). However, the Viton measurements were taken at 200 MHz, at 297 K. They possibly indicate that the motion in the Viton main chains is more restricted than for the copoly(**I**) side chains. For copoly(**I**) in all cases, except for CF_3, the ^{19}F values are shorter than $T_{1\rho}$(H). Similar trends were seen for the Viton $T_{1\rho}$ data of ^{1}H and ^{19}F. The $T_{1\rho}$(F) and $T_{1\rho}$(H) of copoly(**I**) are very similar to those of the major component of the amorphous signal of PVDF (2.9 ms and 5.8 ms respectively[13]).

The analysis of the CP dynamics was done by using the $T_{1\rho}$ data for fluorine and proton as constraints to minimize the number of parameters to be optimised. As mentioned previously, this system is treated as a five-spin-bath problem, whilst strictly speaking there are more baths. Separate measurements for three CF_2 baths were not possible since the resolution was inadequate. As a result, these had to be treated as a single CF_2 bath, referred to as the "internal" CF_2's. Thus an effective CP rate and relative population had to be used for the "internal" CF_2 spin bath. Consequently the relative populations of the "internal" CF_2 do not reflect the stoichiometry of the system properly, being considerably smaller than would be expected. The relative populations of the remaining fluorine spin baths do reflect the stoichiometry of the system, within the uncertainties that can be expected from the deconvolution analysis.

The cross-polarization rates from the proton to the fluorine spin baths reflect the structure of the fluoroalkyl chain. The CP rate from H to CH_2CF_2 is the most rapid at 258 s^{-1}. This decreases to 120 s^{-1} for the internal CF_2 groups and to 97 s^{-1} for the CF_3. The slower CP rate of the CF_3 is in part due to the weakening of dipolar interactions between the protons and the CF_3 arising from rapid rotation about the C–CF_3 bond.

Finite spin-diffusion rates between the fluorine spin baths were required to get reasonable agreement with the experimental data. However, these rates were highly correlated to the cross-polarization rates, as seen in Table 4. Moreover, to obtain statistically independent values for both the spin-diffusion and cross-polarization rates, additional experimental information is required (*e.g.* from inversion–recovery CP[19,20]). In addition, Lee–Goldberg cross-polarization could be used to suppress proton–proton spin diffusion, which perhaps contributes to the fluorine spin-diffusion terms, through a three-stage transfer from F to H, proton spin diffusion, and finally from H back to F. Future work will concentrate on this aspect, since, ideally, the contributions from terms related to fluorine spin diffusion have to be removed in order to evaluate the "true" CP rates.

Conclusions

The theory of cross-polarization dynamics involving multiple (more than two) spin baths has been generalized using the spin-temperature concept. It was implemented in the MATLAB environment for up to six spin baths. The cross-polarization dynamics for a fluoropolymer, copoly(**I**), was studied as a five-spin-bath problem. Separate CP rates and $T_{1\rho}$ values were obtained for each bath. The CP rates from the proton bath to the fluorine baths reflect the side-chain structure. The $T_{1\rho}$'s of the proton bath measured *via* the fluorine signals show little differentiation, indicating rapid ^{1}H spin diffusion. Those of the fluorine baths show significant variation, and are comparable to those of PVDF. The long value for the CF_3 fluorines is attributed to rapid rotation about the C–CF_3 bond and isolation from other fluorines. The cross-polarization rates and the fluorine spin-diffusion rates show significant statistical correlation.

Acknowledgements

The authors thank Professor C.A. Veracini for valuable discussions, the Italian MURST for partial financial support within the framework of PRIN, and EPSRC for financial support (grant GR/M73514). Access to the EPSRC Solid-state NMR Research Service based at Durham is gratefully acknowledged, as is the help in obtaining spectra by Dr. D.C. Apperley and P. Wormald.

References

1 S. Ando, R. K. Harris and S. Reinsberg, *J. Magn. Reson.*, 1999, **141**, 91.
2 M. Mehring, *Principles of High Resolution NMR in Solids*, 2nd edn. of *NMR—Basic Principles and Progress*, vol. 11, Springer-Verlag, Berlin, 1983.
3 B. Gerstein and C. Dybowski, *Transient Techniques in NMR of Solids: An Introduction to Theory and Practice*, Academic Press, London, 1985.
4 P. Holstein, R. K. Harris and B. J. Say, *Solid State Nucl. Magn. Reson.*, 1997, **8**, 201.
5 P. Holstein, U. Scheler and R. K. Harris, *Magn. Reson. Chem.*, 1997, **35**, 647.
6 R. K. Harris, G. A. Monti and P. Holstein, in *Solid State NMR of Polymers*, ed. I. Ando and T. Asakura, Elsevier Science, Amsterdam, 1998, ch. 6.6, pp. 253–266.
7 R. K. Harris, G. A. Monti and P. Holstein, in *Solid State NMR of Polymers*, ed. I. Ando and T. Asakura, Elsevier Science, Amsterdam, 1998, ch. 18, pp. 667–712.
8 P. Holstein, U. Scheler and R. K. Harris, *Polymer*, 1998, **39**, 4937.
9 H. S. Nalwa, *Rev. Macromol. Chem. Phys.*, 1991, **C31**, 341.

10 G. A. Monti and R. K. Harris, *Magn. Reson. Chem.*, 1998, **36**, 892.
11 S. A. Reinsberg, S. Ando and R. K. Harris, *Polymer*, 2000, **41**, 3729.
12 S. Ando, R. K. Harris, P. Holstein, S. A. Reinsberg and K. Yamauchi, *Polymer*, 2001, **42**, 8137.
13 S. Ando, R. K. Harris and S. A. Reinsberg, *Magn. Reson. Chem.*, in the press.
14 N. N. Chuvatkin and I. Yu. Panteleeva, in *Modern Fluoropolymers*, ed. J. Scheirs, Wiley, Chichester, 1997, pp. 191–206; T. Shimizu, in *Modern Fluoropolymers*, ed. J. Scheirs, Wiley, Chichester, 1997, pp. 507–523.
15 R. van de Grampel, *Proceedings of the Symposium Fluoropolymer 2000, Current Frontiers and Future Trends*, Savannah, GA, USA, October 2000.
16 C. M. Kassis, J. K. Steehler, D. E. Betts, Z. Guan, T. J. Romack, J. M. DeSimone and R. W. Linton, *Macromolecules*, 1996, **29**, 3247; Z. Huang, C. Shi, J. Xu, S. Kilic, R. M. Enick and E. J. Beckman, *Macromolecules*, 2000, **33**, 5437.
17 W. H. Press, B. P. Flannery, S. A. Teukolsky and W. T. Vetterling, *Numerical Recipes: The Art of Scientific Computing*, Cambridge University Press, Cambridge, 1986, ch. 14.4, pp. 521–528.
18 E. Katoh, H. Sugimoto, Y. Kita and I. Ando, *J. Mol. Struct.*, 1995, **355**, 21.
19 J. Hirschinger and M. Herve, *Solid State Nucl. Magn. Reson.*, 1994, **3**, 121.
20 P. Reinheimer, J. Hirschinger, P. Gilard and N. Goetz, *Magn. Reson. Chem.*, 1997, **35**, 757.